Solid State Sciences 76 (2018) 111–117

Contents lists available at ScienceDirect

Solid State Sciences

journal homepage: www.elsevier.com/locate/ssscie

Variable-range hopping conductivity in Lu-doped Bi_2Te_3

Oleg Ivanov*, Maxim Yaprintsev

Belgorod State University, Pobedy St., 85, 308015, Belgorod, Russian Federation

ARTICLE INFO

Article history:
Received 1 September 2017
Received in revised form
20 December 2017
Accepted 27 December 2017
Available online 2 January 2018

Keywords:
Bi_2Te_3 semiconductor
Impurity band
Conductivity mechanism
Variable-range hopping conductivity
Magnetoresistance

ABSTRACT

The Seebeck coefficient enhancement due to an increase of density-of-states effective mass of electron has been found in *n*-type $Bi_{1.9}Lu_{0.1}Te_3$. This enhancement is assumed to be related to forming the narrow and non-parabolic impurity (Lu) band with local maximum of electronic density of states lying near the Fermi level. Minimum in the specific electrical resistivity, ρ, originated from change of conductivity mechanism was observed at temperature $T_m \approx 11$ K. Above T_m, the ρ change is due to decrease of electron mobility via acoustic phonon scattering. Below T_m, the variable-range hopping conductivity takes place. The electron hops between the localized states of the impurity energy band occur via tunneling process. Using the temperature and magnetic field dependences of ρ, the localization radius of electron was estimated as $\approx$6 nm. Two parts in the magnetic field dependence of the electrical resistivity were found at temperature of 2 K. At weak magnetic fields, the ρ change is in agreement with the variable-range hopping conductivity mechanism. At high magnetic fields, the positive and almost linear transverse and longitudinal magnetoresistances were observed at low temperatures. Both variable-range hopping conductivity and positive linear magnetoresistance are characteristics of disordered and inhomogeneous semiconductors.

1. Introduction

Element doping is one of prospect and fruitful ways to improve thermoelectric efficiency of materials characterized by the dimensionless thermoelectric figure-of-merit, *ZT* [1–5]. In turn, *ZT* is defined as $(S^2/\rho k)T$, where *T*, *S*, ρ and *k* are the absolute temperature, Seebeck coefficient, specific electrical resistivity and total thermal conductivity. The element doping can at the same time effect on the *S*, ρ and *k* quantities to maximize *ZT*. Atoms or ions of elements forming the narrow and non-parabolic impurity band lying inside or, at least, partially overlapping with conductance (valence) band are the most effective dopants to enhance the thermoelectric figure-of-merit [6–8]. Such kind of impurity band should be characterized by high and sharp density of states (DOS) positioned near the Fermi level. Then, both density-of-states effective mass and scattering factor of carriers can remarkably enhance that in turn results in an increase of the Seebeck coefficient. This doping effect was before used to successfully explain the thermoelectric efficiency improving of PbTe at the Tl doping [9].

Currently, bismuth telluride, Bi_2Te_3, and Bi_2Te_3-based compounds are the best thermoelectric materials for various applications near room temperature [10]. Rare earth elements (Lu, Ce, Sm, Er, La, etc.) used as dopants can enhance the thermoelectric performance of Bi_2Te_3 [11–18]. Forming the narrow and non-parabolic impurity band related to rare earth elements is believed to be one of main sources to enhance *ZT* in this case. According to theoretical predictions, an ideal electronic DOS to maximize the thermoelectric figure-of-merit is the Dirac delta function not achievable in real materials [7,8]. However, electronic *f*-levels of rare earth elements are tightly bound in atoms, and bind little in solids [19]. These levels will give the sharp Lorentzian singularity of very narrow width in DOS near the Fermi level. So, this is the closest approximation to the Dirac delta function.

It is important to note, besides the increase of the Seebeck coefficient, the impurity band can induce other features in the transport properties of thermoelectrics. First of them is a resonance scattering of carriers resulting in extra decrease of a carrier mobility [20]. This feature is due to an electron impulse scattering as electron tunnels from band state to localized one. These electron states have the same energy. The second feature is a hopping conductivity as electron tunnels from one to another localized state within the impurity energy band [21]. The hopping conductivity is characteristic of heavily doped semiconductors, which behave as strongly disordered and inhomogeneous systems. Moreover, the hopping

* Corresponding author.
E-mail address: Ivanov.Oleg@bsu.edu.ru (O. Ivanov).

https://doi.org/10.1016/j.solidstatesciences.2017.12.012
1293-2558/

conductivity is characterized by the specific temperature and magnetic field behavior. Both resonance scattering and hopping conductivity will be observed at low temperatures when acoustic and optical phonon scattering of carriers can be neglected.

The aim of this paper is to find and analyze the features in the temperature and magnetic field dependences of the specific electrical resistivity in $Bi_{1.9}Lu_{0.1}Te_3$ originated from forming the impurity (Lu) band. Undoped Bi_2Te_3 was also studied as reference sample to trace any change of the specific electrical resistivity, Seebeck coefficient and thermoelectric figure-of-merit at the Lu doping. There are two main reasons to choose Lu as dopant. First, Lu was found to be the most effective dopant to enhance the thermoelectric efficiency of Bi_2Te_3 [11]. Second, in contrast to the most of rare earth elements, Lu has zero magnetic moment. So, an additional electron scattering by magnetic moments of impurity atoms will not contribute to the specific electrical resistivity of Lu-doped Bi_2Te_3. In this case, the temperature and magnetic field dependences of the specific electrical resistivity of Bi_2Te_3 at the Lu doping could be analyzed easier and more reliable.

2. Materials and methods

The microwave-solvothermal synthesis and spark plasma sintering were applied to prepare the $Bi_{1.9}Lu_{0.1}Te_3$ and Bi_2Te_3 compounds. In brief, analytically pure chemicals (Bi_2O_3, TeO_2, Lu_2O_3, ethylene glycol, nitric acid and N,N-dimethylformamide) were used for the synthesis. First, the oxides taken in a stoichiometric ratio for each compound were dissolving in mixture of concentrated nitric acid and ethylene glycol. Then, N,N-dimethylformamide was added in mixture after dissolving. The microwave-assisted reaction was carried out in a MARS-6 microwave reactor for 15 min at pressure of 4 MPa and temperature of 463 K. To sinter the bulk $Bi_{1.9}Lu_{0.1}Te_3$ and Bi_2Te_3 samples, spark plasma sintering method was applied by using a SPS-25/10 system at pressure of 40 MPa, temperature of 683 K and sintering time of 5 min.

The densities of the bulk samples were measured by the Archimedes' method.

To characterize both structure and phase compositions of the bulk $Bi_{1.9}Lu_{0.1}Te_3$ and Bi_2Te_3 compounds, X-ray diffraction (XRD) analysis was performed by a Rigaku Ultima IV diffractometer with CuK_α − radiation.

Energy dispersive X-ray spectroscopy (EDX) method by using scanning electron microscope a Nova NanoSEM 450 was applied to map the Lu distribution in $Bi_{1.9}Lu_{0.1}Te_3$.

The specific electrical resistivity, ρ, and Seebeck coefficient, S, above room temperature were measured by using a ZEM-3 system. The S and ρ values along with the thermal conductivity value, k, were further used to calculate the thermoelectric figure-of-merit value. To determine k by the laser flash method, a TC-1200 system was applied.

The temperature and magnetic field dependences of the specific electrical resistivity at low temperatures were taken by a Cryogenic Free system. This system was also used to study the Hall effect and extract the type, concentration, n, and Hall mobility, μ_H, of the majority charge carriers.

3. Results and discussion

3.1. The samples characterization

The XRD patterns for the bulk Bi_2Te_3 and $Bi_{1.9}Lu_{0.1}Te_3$ compounds taken at room temperature are shown in Fig. 1. According to the XRD analysis, these compounds are single hexagonal phase characteristic for pure Bi_2Te_3. The Lu atoms are believed to incorporate to the Bi_2Te_3 lattice changing the lattice parameters. The lattice "a" and "c" parameters calculated by the Rietveld refinement are equal to 4.385 Å and 30.476 Å for Bi_2Te_3 and 4.388 Å and 30.481 Å for $Bi_{1.9}Lu_{0.1}Te_3$, respectively. Details of the Rietveld refinement are shown in Supplementary Fig. S1 (Bi_2Te_3) and Fig. S2 ($Bi_{1.9}Lu_{0.1}Te_3$). In fact, the "a" and "c" changes are very small and close to an accuracy of the XRD analysis. So, just weak effect of the Lu doping on the Bi_2Te_3 structure could be founded in XRD phases. Weakness of this effect should be attributed to a small difference between ionic radii of Lu (1.001 Å) and bismuth (1.100 Å) [22].

To confirm uniformity of the Lu distribution in $Bi_{1.9}Lu_{0.1}Te_3$, the EBSD method was applied (Fig. 1 (b) and (c)). One can see from the EBSD mapping that Lu is uniformly distributed.

The densities of the Bi_2Te_3 and $Bi_{1.9}Lu_{0.1}Te_3$ samples were equal to 6.72 g/cm^3 and 6.82 g/cm^3, respectively, which are 87% and 88.5% of the theoretical density of Bi_2Te_3 (7.7 g/cm^3). So, the densities of these samples were less than the theoretical density. However, it is important to note these densities are almost the same for both compounds. Then, the expected effect of porosity on the transport properties of the samples under study should be the same, too. In this case, any changes in the transport properties of Lu-doped Bi_2Te_3 should be attributed to the Lu doping.

3.2. The specific electrical resistivity and Seebeck coefficient above room temperature

First of all, let us analyze the ρ and S changes in Bi_2Te_3 originated from the Lu doping. To do so, the type, concentration and Hall mobility of the majority charge carriers for both $Bi_{1.9}Lu_{0.1}Te_3$ and Bi_2Te_3 were firstly determined. According to the Hall effect study, the majority charge carriers for both compounds are electrons. Values of the electron concentration and electron Hall mobility taken at room temperature are listed in Table 1.

The type and concentration of carriers in Bi_2Te_3 are closely related to point defects [1,2]. The most common point defects are vacancies at the Te sites (V_{Te}, provides two electrons per defect), vacancies at the Bi sites (V_{Bi}, contributes three holes per defect) and antisite defects of Bi at the Te sites (Bi_{Te}, is accompanied with formation of one hole). Besides, for polycrystalline Bi_2Te_3, the dangling bonds at grain boundaries due to Te deficiencies can be considered as fractional-V_{Te} working as n-type dopants in the same manner as whole-V_{Te} defects inside the grains. Therefore, polycrystalline undoped Bi_2Te_3 can behave as an n-type semiconductor due to dangling bonds at grain boundaries and V_{Te} vacancies.

According to Table 1, the Lu doping results in the n increase and μ_H decrease. The doping effect on n is related to the difference of electronegativity for elements forming the antisite Bi_{Te} defects responsible for appearance of holes. The electronegativity values are equal to 2.1, 2.02 and 1.27 for Te, Bi and Lu, respectively. So, a larger electronegative difference for the Lu-Te pair as compared with the Bi-Te pair will decrease the concentration of antisite defects at the Te-sites which contributes one hole per defect and hence results in more electrons.

Reducing the carrier mobility in Bi_2Te_3 can be originated from an alloy scattering of carriers due to the Lu doping [23,24]. The alloy scattering is related to forming the point defects in the Bi_2Te_3 lattice as a result of substituting the Lu atoms for the Bi sites.

The $\rho(T)$ dependences for $Bi_{1.9}Lu_{0.1}Te_3$ and Bi_2Te_3 taken within the 285–450 K range are presented in Fig. 2 (a).

As is seen, ρ of these compounds increases with increasing temperature. This behavior is typical for degenerate semiconductors and metals [25]. The specific electrical resistivity of solids is expressed as $\rho = 1/(en\mu)$, where e is the charge of electron. The $\rho(T)$ behavior of the degenerate semiconductors is determined by T-dependent μ contribution, while n contribution is T-independent. The electron mobility due to phonon scattering of carriers

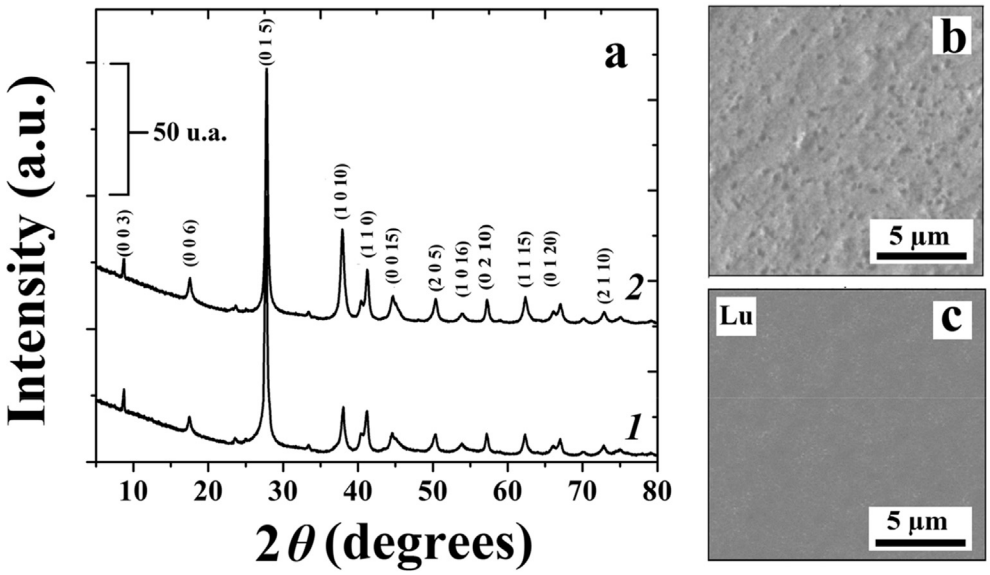

Fig. 1. (a) XRD patterns of Bi_2Te_3 (*1*) and $Bi_{1.9}Lu_{0.1}Te_3$ (*2*); (b) SEM image of the $Bi_{1.9}Lu_{0.1}Te_3$ surface; (c) EBSD mapping of Lu on the $Bi_{1.9}Lu_{0.1}Te_3$ surface.

Table 1
The concentration (n), Hall mobility (μ_H) and density-of-states effective mass of electrons (m^*) in Bi_2Te_3 and $Bi_{1.9}Lu_{0.1}Te_3$.

Compound	n (10^{19}, cm^{-3})	μ_H ($cm^2 \cdot V^{-1} \cdot s^{-1}$)	m^*
Bi_2Te_3	1.2	420	$0.16m_0$
$Bi_{1.9}Lu_{0.1}Te_3$	2.4	360	$0.25m_0$

can be described by empirical expression [26].

$$\mu \sim T^{-m}, \tag{1}$$

where m is an exponent changing from 1.5 up to 2.5. For acoustic phonon scattering acting as main scattering mechanism at low temperatures, m is equal to 1.5. Above the Debye temperature, optical phonon scattering becomes comparable to acoustic phonon scattering and m increases towards 2.5. For instance, the electron mobility for n-type silicon varies as $T^{-2.3}$ when both optical and acoustic phonon scattering become dominant. The Debye temperature for Bi_2Te_3 is equal to ~150 K. Inset to Fig. 2 (a) shows that the best fit for the experimental $\rho(T)$ curves corresponds to $m = 2.2$. Thus, the scattering mechanism is the same for both Bi_2Te_3 and $Bi_{1.9}Lu_{0.1}Te_3$.

Hence, although the alloy scattering reduces the μ value in Lu-doped Bi_2Te_3 (Table 1), the $\rho(T)$ dependences in Fig. 2 (a) are determined by optical and acoustic phonon scattering, rather than by the alloy scattering. The matter is that the alloy scattering is one of mechanisms determining the low-temperature electrical conductivity of solids. It becomes dominant when the phonon scattering can be neglected. Due to the alloy scattering, at low temperatures ρ will be T-independent when electron scattering by neutral impurities takes place or will vary as $T^{3/2}$ when ionized impurities act as scattering centres.

The $S(T)$ dependences for Bi_2Te_3 and $Bi_{1.9}Lu_{0.1}Te_3$ are shown in Fig. 2 (b). Since the majority charge carries are electrons, the Seebeck coefficient has a negative sign. The $S(T)$ dependences are parallel to each other and linearly increase with increasing temperature. The Seebeck coefficient of the degenerate semiconductors can be expressed as [11].

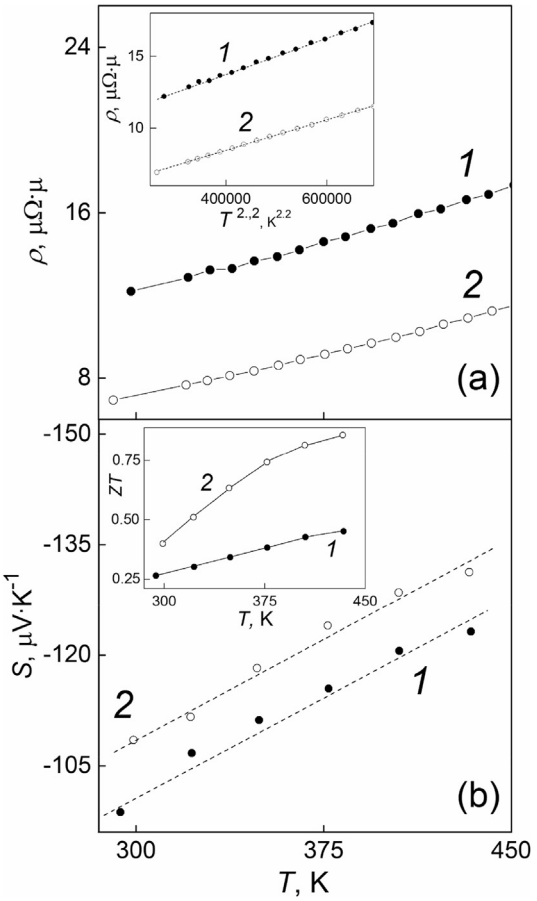

Fig. 2. The ρ vs. T (a) and S vs. T (b) dependences for Bi_2Te_3 (curve *1*) and $Bi_{1.9}Lu_{0.1}Te_3$ (*2*). Insets to Figures: the ρ vs. $T^{2.2}$ (a) and ZT vs. T (b) dependences for the same compounds.

$$S = \frac{2k_B^2 T m^*}{3e\hbar^2}\left(\frac{\pi}{3n}\right)^{2/3}\left(\frac{3}{2}+\gamma\right), \quad (2)$$

where k_B is the Boltzmann constant, $\hbar$ is the reduced Planck constant, m^* is the density-of-states effective mass of electron and γ is the scattering factor.

Expression (2) shows that a higher n decreases S, while a larger γ increases the Seebeck coefficient. Normally, the ρ increase is accompanied by the S increase. But, Fig. 2 (b) shows an opposite trend. So, the possible m^* and γ changes in addition to the n change should be taken into account to explain the S behavior in Bi_2Te_3 at the Lu doping. The γ value is determined by mechanism of the charge carriers scattering. According to the inset to Fig. 2 (a), this mechanism is the same for all the compounds studied. So, γ will be the same, too. The γ value is equal to $-1/2$ for acoustic phonon scattering and 0 for optical phonon scattering above the Debye temperature [27,28]. As was discussed above, both optical and acoustic phonon scattering should be considered as the dominant mechanisms to account for the $\rho(T)$ behaviour in Fig. 2 (a). Therefore, for further S analysis, let us assume that $\gamma = -1/2$ (acoustic phonon scattering) + 0 (optical phonon scattering) = $-1/2$. Next, in accordance with expression (2), a rate of the linear $S(T)$ growth in Fig. 2 (b) is characterized by a coefficient $\Delta S[\mu V \cdot K^{-1}]/\Delta T$ [K] $\approx 2.14 \times 10^{-7}$. Using the n (Table 1), $\Delta S/\Delta T$ and γ values, the density-of-states effective mass of electron can be estimated. The m^* estimates are listed in Table 1 (m_0 is mass of free electron). So, at the Lu doping m^* substantially increases from $0.16m_0$ for undoped Bi_2Te_3 up to $0.25m_0$ for $Bi_{1.9}Lu_{0.1}Te_3$.

As was mentioned above, the m^* increase can be related to forming the narrow and non-parabolic Lu band with the high and sharp DOS near the Fermi level. For instance, schematic diagram showing the narrow and non-parabolic impurity band lying inside conduction band in an n-type semiconductor is presented in Supplementary Fig. S3.

Effect on electronic structure on the Seebeck coefficient is partly explained by Motts equation

$$S = \frac{\pi^2 k_B^2 T}{3e}\frac{dln(\sigma(E))}{dE}_{E=E_F}, \quad (3)$$

where $\sigma(E)$ is the electronic conductivity as a function of the Fermi energy, E_F.

As $\sigma(E) = n(E)\cdot e\cdot\mu(E)$ and $n(E) = g(E)f(E)$, expression (3) can be rewritten as

$$S = \frac{\pi^2 k^2 T}{3e}\left\{\frac{1}{\mu}\frac{d\mu(E)}{dE} + \frac{1}{g(E)f(E)}\frac{dg(E)f(E)}{dE}\right\}_{E=E_F}, \quad (4)$$

where $g(E)$ is the electronic DOS and $f(E)$ is the Fermi function.

So, rapidly changing DOS near E_F (Fig. 3) will result in larger S than flatter DOS near E_F. That is, the Seebeck coefficient can be considered as a measure of asymmetry in the electronic structure and scattering rates near the Fermi level. Disturbances in the electronic structure and scattering rates within a narrow energy interval near E_F can induce such kind of asymmetry. According to expression (4), the Seebeck coefficient can be increased via increasing the energy dependences of $\mu(E)$ or $n(E)$. The $\mu(E)$ dependence can be increased by a specific scattering mechanism that strongly depends on energy of electrons, while the $n(E)$ dependence can be increased by a local increase in DOS. The Mahan-Sofo theory [8] suggests that such local increase in DOS due to the narrow and non-parabolic impurity band will enhance the Seebeck coefficient.

It is important to note that the thermoelectric figure-of-merit of

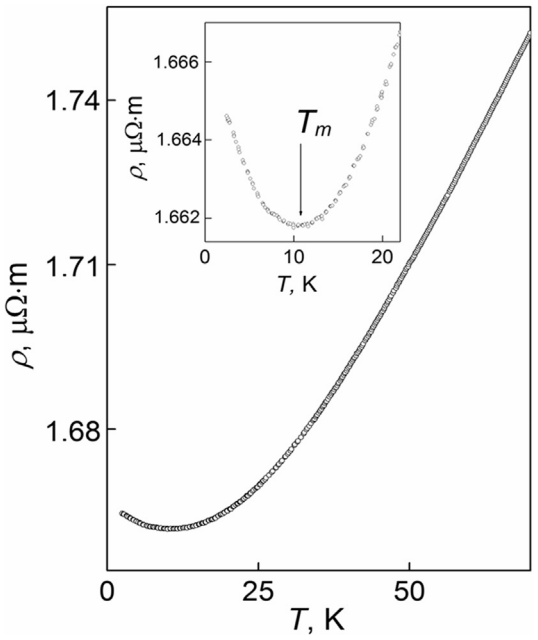

Fig. 3. The ρ vs. T dependence for $Bi_{1.9}Lu_{0.1}Te_3$. Inset: the $\rho(T)$ minimum at $T_m \approx 11$ K.

Bi_2Te_3 is sufficiently increasing at the Lu doping (inset to Fig. 2 (b)). To calculate the ZT values, the S and ρ were used (Fig. 2 (a) and (b)) and the thermal conductivities of the Lu-doped and undoped samples were measured. The enhancement of the Seebeck coefficient via increase of the density-of-states effective mass for conduction band is one of main origins resulting in the ZT increase in doped Bi_2Te_3.

3.3. The electrical conductivity mechanisms at low temperatures

Thus, the S enhancement in Lu-doped Bi_2Te_3 could be originated from forming the Lu band. As was mentioned above, the features of low-temperature transport properties should be observed in this case. The $\rho(T)$ dependence for $Bi_{1.9}Lu_{0.1}Te_3$ taken within the 2–70 K range is shown in Fig. 3.

Clear $\rho(T)$ minimum is observed at temperature $T_m \approx 11$ K as shown in inset to Fig. 3. Above this temperature, ρ increases with increasing temperature demonstrating again the behaviour typical for degenerate semiconductors or metals. Below T_m, the $\rho(T)$ dependence is typical for semiconductors that is ρ increases with decreasing temperature. The $\rho(T)$ minimum is obviously related to the change of the conductivity mechanism from "metal" type to "semiconductor" one. It was found the $\rho(T)$ dependence varies as $T^{3/2}$ above T_m starting from temperature $T_d \approx 30$ K up to 70 K (Fig. 4).

This temperature behavior is determined by the temperature dependence of the electron mobility due to only acoustic phonon scattering as the dominant scattering mechanism working below the Debye temperature. Then, the electron mobility can be written as

$$\mu_n = \frac{2\sqrt{2\pi}\, e\hbar^2 d v_s^2}{3m^{*5/2}(k_B T)^{3/2} D_{ac}^2}, \quad (5)$$

where d is the mass density, υ_s is the sound velocity and D_{ac} is the deformation potential.

It should be noted no $\rho(T)$ minimum observed in undoped Bi_2Te_3. So, the Lu doping is responsible for appearance of this minimum. There are several mechanisms resulting in the

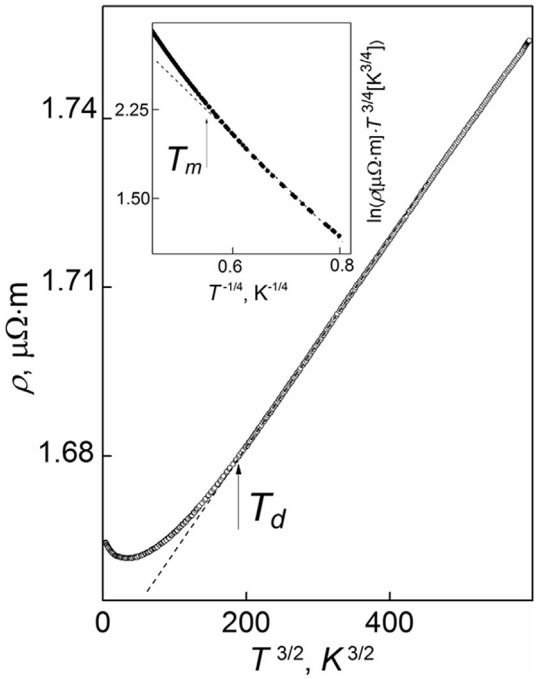

Fig. 4. The ρ vs. $T^{3/2}$ dependence for $Bi_{1.9}Lu_{0.1}Te_3$. Inset: the $\ln(\rho \cdot T^{3/4})$ vs. $T^{-1/4}$ dependence.

"semiconductor" type $\rho(T)$ behavior observed below T_m. The main mechanisms are the scattering by neutral or ionized impurities [26], Kondo effect [29], electron-electron scattering [30], and hopping conductivity [21]. Of these mechanisms, the hopping conductivity is the most attractive and interesting mechanism to explain the low-temperature transport properties of heavily doped semiconductors with the impurity energy band creating the local maximum in the electronic DOS. Therefore, let us try to describe the $\rho(T)$ dependence below T_m (Fig. 3) in framework of the hopping conductivity mechanism.

The hopping conductivity in three dimensional doped crystalline semiconductors can be realized via different mechanisms given by a universal equation [31].

$$\rho(T) = \rho_0(T) exp\left[\left(\frac{T_0}{T}\right)^p\right], \tag{6}$$

where $\rho_0(T)$ is the pre-exponential factor, T_0 is the characteristic temperature and p is the exponent depending on the hopping conductivity mechanism.

The case of $p = 1$ corresponds to the regime of nearest-neighbor hopping conductivity and $p = 1/4$ and $1/2$ to the Mott and Shklovskii-Efros types of variable-range hopping (VRH) conductivity, respectively [31]. Generally, the VRH conductivity sets in when the internal microscopic disorder is high enough to make tunneling between the nearest sites energetically unfavorable.

If the $\rho(T)$ change due to the hopping conductivity is strong enough, the $\rho_0(T)$ contribution to total $\rho(T)$ dependence can be neglected, i.e. only exponential factor can be taken into account in equation (6). But, if ρ changes weakly, both pre-exponential and exponential factors should be taken into account at the same time. For $Bi_{1.9}Lu_{0.1}Te_3$, the $\rho(T)$ change observed around T_m is very weak. So, the $\rho_0(T)$ factor is also significant one. This factor can be expressed as [32].

$$\rho_0(T) = AT^q, \tag{7}$$

where A is the constant and q is the exponent depending on the regime of the hopping conductivity.

It was found the best fit for the experimental $\rho(T)$ curve below T_m corresponds to $p = 1/4$ and $q = -3/4$ (inset to Fig. 4). Such p value is characteristic of the VRH conductivity of the Mott type, and such q value is related to wave function for localized electron expressed as [31].

$$\psi(r) \sim r^{-1} exp\left(-\frac{r}{a}\right), \tag{8}$$

where a is the localization radius of electron.

The characteristic temperature T_0 estimated from a slope of the $\ln(\rho \cdot T^{3/4})$ vs. $T^{-1/4}$ line in inset to Fig. 4 is equal to ≈ 370 K.

3.4. Low-temperature magnetoresistance

Thus, the VRH conductivity of the Mott type can be responsible for the $\rho(T)$ change in $Bi_{1.9}Lu_{0.1}Te_3$ below T_m. Besides the specific $\rho(T)$ dependence, the VRH conductivity is also characterized by the specific magnetic field dependence, $\rho(H)$. It is known [21] both $\rho(T)$ and $\rho(H)$ dependences for the VRH conductivity can be expressed by a single equation

$$ln\frac{\rho(H)}{\rho(0)} = t_1\left(\frac{a}{L_H}\right)^4\left(\frac{T_0}{T}\right)^{3/4}, \tag{9}$$

where t_1 is the constant equal to 5/2016 and L_H is the magnetic length.

In turn, L_H is defined as

$$L_H = \left(\frac{c\hbar}{eH}\right)^{1/2}, \tag{10}$$

where c is the speed of light.

The magnetic field dependences of the transverse and longitudinal magnetoresistance, $\rho(H)/\rho(0)$, for $Bi_{1.9}Lu_{0.1}Te_3$ taken at temperature of 2 K are shown in Fig. 5 (a). Here, $\rho(H)$ is the specific electrical resistivity at magnetic field H changing from 0 up to 40 kOe, and $\rho(0)$ is the specific electrical resistivity at zero magnetic field. Magnetic field was applied perpendicular to current direction to measure the transverse magnetoresistance, while parallel orientation of magnetic field and current direction was used to measure the longitudinal magnetoresistance.

As is seen in Fig. 5 (a), $Bi_{1.9}Lu_{0.1}Te_3$ is characterized by the positive magnetoresistance, since both transverse and longitudinal $\rho(H)/\rho(0)$ dependences increase as magnetic field increases. The transverse magnetoresistance magnitude is about twice more than the longitudinal magnetoresistance magnitude. It is important to note that both $\rho(H)/\rho(0)$ dependences do not saturate up to maximum H value. These dependences can be divided into two parts. At weak magnetic fields, ρ rapidly increases with increasing magnetic field up to some crossover field, H_C. But, the $\rho(H)/\rho(0)$ vs. H dependences very close to linear take place at higher magnetic fields above H_C. The crossover fields, $H_{\perp C}$ and $H_{\parallel C}$, are equal to ≈ 20 kOe for both transverse and longitudinal magnetoresistance. Two parts in the $\rho(H)/\rho(0)$ curves corresponding to the weak and high magnetic fields can be very clearly demonstrated by the derivative $d[\rho(H)/\rho(0)]/dH$ vs. H dependence as shown for the transverse magnetoresistance in Fig. 5 (b). These two parts are really different in the rate of the $\rho(H)$ change.

It should be noted that the positive linear magnetoresistance is

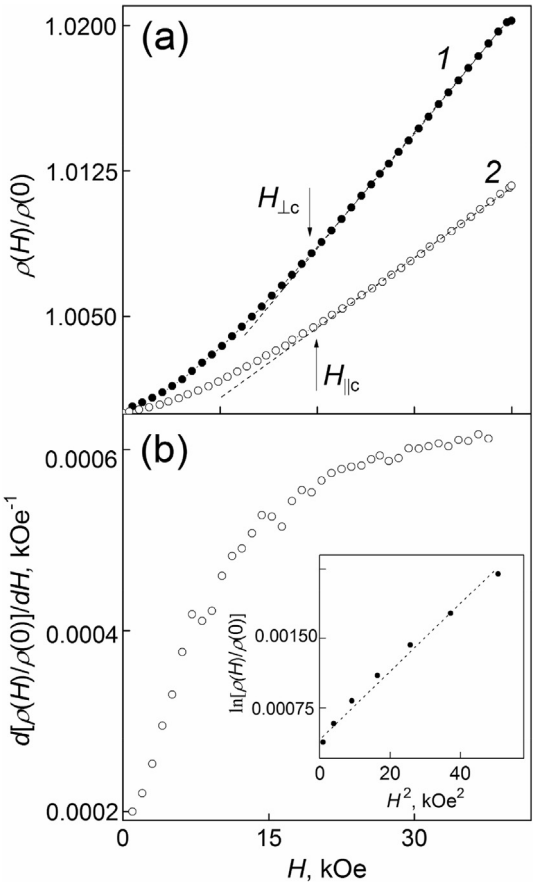

Fig. 5. (a) The transverse (curve *1*) and longitudinal (*2*) $\rho(H)/\rho(0)$ vs. H dependences for $Bi_{1.9}Lu_{0.1}Te_3$ at temperature of 2 K. (b) The $d[\rho(H)/\rho(0)]/dH$ vs. H dependence for the transverse magnetoresistance. Inset: the $\ln[\rho(H)/\rho(0)]$ vs. H^2 dependence.

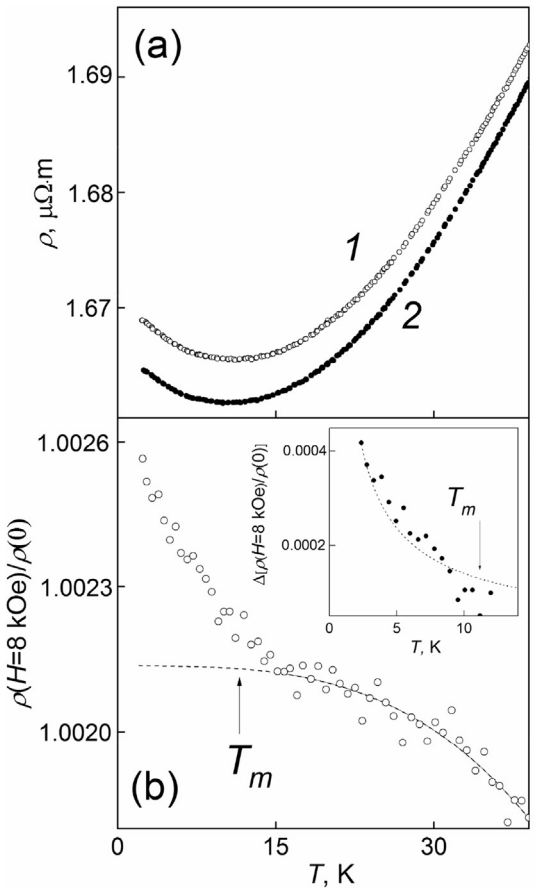

Fig. 6. (a) The $\rho(H = 8$ kOe) - curve *1* and $\rho(0)$ – *2* vs. T dependences in $Bi_{1.9}Lu_{0.1}Te_3$. (b) The $\rho(H = 8$ kOe)/$\rho(0)$ vs. T dependence. Dashed curve is a background change. Inset: the $\Delta\rho[(H = 8$ kOe)/$\rho(0)]$ vs. T dependence (dashed curve varies as $T^{3/4}$).

often observed in the inhomogeneous and disordered semiconductors [33–35]. In turn, the VRH conductivity assumed for $Bi_{1.9}Lu_{0.1}Te_3$ in our experiments is also characteristic of such kind of semiconductors. Moreover, the transverse magnetoresistance magnitude is usually much more than the longitudinal magnetoresistance magnitude. But, the magnitudes of the transverse and longitudinal magnetoresistances are comparable for $Bi_{1.9}Lu_{0.1}Te_3$. This feature can also be related to strong disorder and inhomogeneity of Lu-doped Bi_2Te_3.

The magnetic field $\rho(H)/\rho(0)$~H^2 dependence is known to be typical for a lot of conventional metals and semiconductors and associated with cyclotron motion of carriers under external magnetic field [36]. However, for semiconductors with the VRH conductivity, the field $\ln[\rho(H)/\rho(0)]$~H^2 dependence would be more correct to describe the experimental $\rho(H)$ curves (expression (9)). Actually, at weak magnetic fields the $\rho(H)/\rho(0)$ vs. H dependence can be satisfactory described by expression (9), because the replotted $\ln[\rho(H)/\rho(0)]$ vs. H^2 dependence is close enough to line (inset to Fig. 5 (b)). In this case, a rate of linear growth is characterized by a coefficient $\Delta\ln[\rho(H)/\rho(0)]/\Delta H^2[\text{kOe}^2] \approx 3.7 \times 10^{-11}$. Then, using the values of this coefficient and temperature T_0, expression (9) was applied to estimate the localization radius a. The estimate is equal to ≈6 nm.

To extract the temperature $\rho(H)$ behavior due to the VRH conductivity in $Bi_{1.9}Lu_{0.1}Te_3$, the temperature $\rho(H = 8$ kOe) and $\rho(0)$ dependences were taken within the 2–40 K range (Fig. 6 (a)). The transverse magnetoresistance orientation was applied in this experiment. Next, the temperature dependence of the $\rho(H = 8$ kOe)/$\rho(0)$ magnetoresistance was plotted (Fig. 6 (b)). As is seen, $\rho(H = 8$ kOe)/$\rho(0)$ increases with decreasing temperature and a clear upwards deviation takes place below T_m. A background $\rho(H = 8$ kOe)/$\rho(0)$ change above T_m was described by empirical expression

$$\rho(H = 8\text{ kOe})/\rho(0) = 1.002\ [\mu\Omega\cdot\text{m}] - 1.8 \times 10^{-9}\left[(\mu\Omega\cdot\text{m})\cdot\text{K}^{-3}\right] \times T^3, \quad (11)$$

as shown by dashed line in Fig. 6 (a).

By subtracting the background change from the $\rho(H = 8$ kOe)/$\rho(0)$ vs. T curve, the VRH conductivity contribution to total magnetoresistance was recovered (inset to Fig. 6 (b)). In accordance with expression (9), this contribution should be varied as $T^{3/4}$. Dashed curve in inset corresponds to this T-variation.

Results of detailed magnetoresistance examination of Lu-doped Bi_2Te_3 will be published elsewhere.

4. Conclusion

So, it is found the Lu doping results in the Seebeck coefficient enhancement of Bi_2Te_3 via an increase of density-of-states effective mass of electron. This enhancement can be originated from forming the narrow and non-parabolic Lu band with local maximum of the electronic DOS near the Fermi level. The variable-range hopping conductivity with the localization radius of ≈6 nm was observed at

low temperatures below $T_m \approx 11$ K. The electron hops between the localized states of the impurity energy band take place via tunneling process. The magnetoresistance features typical for disordered and inhomogeneous semiconductors are also in agreement with the hopping conductivity mechanism.

Acknowledgements

This work was also financially supported by the Ministry of Education and Science of the Russian Federation under project No 3.6586.2017/BY.

Appendix A. Supplementary data

Supplementary data related to this article can be found at https://doi.org/10.1016/j.solidstatesciences.2017.12.012.

References

[1] Y. Pan, T.R. Wei, C.F. Wu, J.F. Li, Electrical and thermal transport properties of spark plasma sintered n-type $Bi_2Te_{3-x}Se_x$ alloys: the combined effect of point defect and Se content, J. Mater. Chem. C 3 (2015) 10583–10589.
[2] L. Hu, T. Zhu, X. Liu, X. Zhao, Point defect engineering of high-performance bismuth-telluride-based thermoelectric materials, Adv. Funct. Mater. 24 (2014) 5211–5218.
[3] J. Suh, K.M. Yu, D. Fu, X. Liu, F. Yang, J. Fan, D.J. Smith, Y.H. Zhang, J.K. Furdyna, C. Dames, W. Walukiewicz, J. Wu, Simultaneous Enhancement of electrical conductivity and thermopower of Bi_2Te_3 by multifunctionality of native defects, Adv. Mater. 27 (2015) 3681–3686.
[4] S. Saini, H.S. Yaddanapudi, K. Tian, Y. Yin, D. Magginetti, A. Tiwari, Terbium ion doping in $Ca_3Co_4O_9$: a step towards high-performance thermoelectric materials, Sci. Rep. 7 (2017), 44621–1-7.
[5] R.R. Sun, X.Y. Qin, L.L. Li, D. Li, J. Zhang, S. Zhang, C.J. Tang, The effects of elements doping on transport and thermoelectric properties of $Sr_3Ti_2O_7$, J. Phys. Chem. Phys. Sol 75 (2014) 629–637.
[6] H.J. Goldsmid, Impurity band effects in thermoelectric materials, J. Electron. Mater. 41 (2012) 2126–2129.
[7] T.E. Hupphrey, H. Linke, Reversible thermoelectric nanomaterials, Phys. Rev. Lett. 94 (2005) 096601–096604.
[8] G.D. Mahan, J.O. Sofo, The best thermoelectric, Pros. Natl. Acad. Sci. USA 93 (1996) 7436–7439.
[9] J.P. Heremans, V. Jovovic, E.S. Toberer, A. Saramat, K. Kurosaki, A. Charoenphakdee, S. Yamanaka, G.J. Snyder, Enhancement of thermoelectric efficiency in PbTe by distortion of the electronic density of states, Science 321 (2008) 554–557.
[10] G. Mahan, B. Sales, J. Sharp, Thermoelectric materials: new approaches to an old problem, Phys. Today 50 (1997) 42–47.
[11] J. Yang, F. Wu, Z. Zhu, L. Yao, H. Song, X. Hu, Thermoelectrical properties of lutetium-doped Bi_2Te_3 bulk samples prepared from flower-like nanopowders, J. Alloys Compd. 619 (2015) 401–405.
[12] X.H. Ji, X.B. Zhao, Y.H. Zhang, B.H. Lu, H.L. Ni, Synthesis and properties of rare earth containing Bi_2Te_3 based thermoelectric alloys, J. Alloys Compd. 387 (2005) 282–286.
[13] F. Wu, H. Song, J. Jia, X. Hu, Effects of Ce, Y,and Sm doping on the thermoelectric properties of Bi_2Te_3 alloy, Prog. Nat. Sci. Mater. Int. 23 (2013) 408–412.
[14] F. Wu, W. Shi, X. Hu, Preparation and thermoelectric properties of flower-like nanoparticles of Ce-Doped Bi_2Te_3, Electron. Mater. Lett. 11 (2015) 127–132.
[15] X.H. Ji, X.B. Zhao, Y.H. Zhang, B.H. Lu, H.L. Ni, Solvothermal synthesis and thermoelectric properties of lanthanum contained Bi–Te and Bi–Se–Te alloys, Mater. Lett. 59 (2005) 682–685.
[16] F. Wu, H.Z. Song, J.F. Jia, F. Gao, Y.J. Zhang, X. Hu, Thermoelectric properties of Ce-doped n-type $Ce_xBi_{2-x}Te_{2.7}Se_{0.3}$ nanocomposites, Phys. Stat. Sol. A 210 (2013) 1183–1189.
[17] W.Y. Shi, F. Wu, K.L. Wang, J.J. Yang, H.Z. Song, X.J. Hu, Preparation and thermoelectric properties of yttrium-doped Bi_2Te_3 flower-like nanopowders, Electron. Mater 43 (2014) 3162–3168.
[18] X.B. Zhao, Y.H. Zhang, X.H. Ji, Solvothermal synthesis of nano-sized La_x-$Bi_{(2-x)}Te_3$ thermoelectric powders, Inorg. Chem. Commun. 7 (2004) 386–388.
[19] M.D. Daybell, W.A. Steyert, Localized magnetic impurity states in metals: some experimental relationships, Rev. Mod. Phys. 40 (1968) 380–389.
[20] Y.I. Ravich, Handbook of Thermoelectrics, CRC Press, Boca Raton, FL, 1995.
[21] B.I. Shklovskii, A.L. Efros, Electronic Properties of Doped Semiconductor, Springer, Berlin, 1984.
[22] Y.Q. Jia, Crystal radii and effective ionic radii of the rare earth ions, J. Sol. State Chem. 95 (1991) 184–187.
[23] D.C. Look, D.K. Lorance, J.R. Sizelove, C.E. Stutz, K.R. Evans, D.W. Whitson, Alloy scattering in p-type $Al_xGa_{1-x}As$, J. Appl. Phys. 71 (1992) 260–266.
[24] H.S. Bennett, Majority and minority electron and hole mobilities in heavily doped gallium aluminium arsenide, J. Appl. Phys. 80 (1996) 3844–3853.
[25] K. Behnia, Fundamentals of Thermoelectricity, Oxford University Press, Oxford, 2015.
[26] D.A. Neamen, Semiconductor Physics and Devices, McGraw-Hill New York, 2012.
[27] W.S. Liu, L.D. Zhao, B.P. Zhang, H.L. Zhang, J.F. Li, Enhanced thermoelelctric property originating from additional carrier pocket in scutterudite compounds, Appl. Phys. Lett. 93 (2008), 042109–1-4.
[28] W. Liu, X. Yan, G. Chen, Z. Ren, Recent advances in thermoelectric nanocomposites, Nano Energy 1 (2012) 42–56.
[29] B. Huard, A. Anthore, N.O. Birge, H. Pothier, D. Esteve, Effect of magnetic impurities on energy exchange between electrons, Phys. Rev. Lett. 95 (2005), 036802–1-4.
[30] M.W. Swift, C.G. Van de Walle, Conditions for T^2 resistivity from electron-electron scattering, Eur. Phys. J. B 90 (2017) 151.
[31] R. Laiho, A.V. Lashkul, K.G. Lisunov, E. Lahderanta, M.A. Shakhov, V.S. Zakhvalinskii, Hopping conductivity of Ni-doped p-CdSb, J. Phys. Condens. Mater 20 (2008), 295204–1-8.
[32] R. Laiho, K.G. Lisunov, E. Lahderanta, P.A. Petrenko, J. Salminen, M.A. Shakhov, M.O. Safontchik, V.S. Stamov, M.V. Shybnikov, V.S. Zakhvalinskii, Variable-range hopping conductivity in $La_{1-x}Ca_xMn_{1-y}Fe_yO_3$: evidence of a complex gap in density of states near the Fermi level, J. Phys. Condens. Mater 14 (2002) 8043–8055.
[33] R. Xu, A. Husmann, T.F. Rosenbaum, M.L. Saboungi, J.E. Enderby, P.B. Littlewood, Large magnetoresistance in non-magnetic silver chalcogenides, Nature 390 (1997) 57–60.
[34] A. Husmann, J.B. Betts, G.S. Boebinger, A. Migliori, T.F. Rosenbaum, M.L. Saboungi, Megagauss sensors, Nature 417 (2002) 421–424.
[35] J. Hu, T.F. Rosenbaum, Quantum and classical routes to linear magnetoresistance, Nature Matl 7 (2008) 697–700.
[36] A.B. Pippard, Magnetoresistance in Metals, Cambridge University, Cambridge, 1989.